Journal of
Materials Chemistry A

Materials for energy and sustainability

Accepted Manuscript

This article can be cited before page numbers have been issued, to do this please use: J. Sun, Y. Xu and J. Kainz, *J. Mater. Chem. A*, 2026, DOI: 10.1039/D6TA03434A.

ROYAL SOCIETY OF CHEMISTRY

rsc.li/materials-a

View Article Online
DOI: 10.1039/D6TA03434A

Protocol-aware standardization of relaxation-induced kinetic masking in incremental capacity fingerprints of lithium-ion batteries

Received 00th January 20xx,
Accepted 00th January 20xx

DOI: 10.1039/x0xx00000x

Jinghua Sun[a,b] , Yaolin Xu *[a], Josef Kainz [b,c]

Incremental capacity analysis (ICA) is widely used to probe lithium-ion battery degradation because it preserves material-related information in the voltage response. Its mechanistic value, however, depends on whether the measured voltage trajectory provides a comparable projection of electrode phase responses, polarization, and transport limitations. Here, we show that insufficient pre-charge relaxation introduces a relaxation-induced kinetic masking that can distort ICA fingerprints before material-related interpretation. A controlled-aging dataset of 12 commercial NMC-type 21700 cells and 166 reference performance tests was used, in which four ICA-related charges with 60, 30, 10, and 0 min of pre-charge relaxation were repeatedly conducted under otherwise identical conditions within each test. Short relaxation first shifts the charging-voltage trajectory and then amplifies this deviation in the dQ/dU domain, producing peak displacement, centroid drift, and area redistribution within reproducible fingerprint windows. The distortion depends systematically on charge rate, depth of discharge, state of health, and voltage window, indicating that it is a structured non-equilibrium projection. To mitigate this protocol-induced masking, we developed a voltage-domain relaxation lens based on an effective voltage-dependent relaxation timescale, τ(U), a compact, effective descriptor of the transferable relaxation-induced voltage bias in the voltage domain. The framework does not aim to recover an ideal equilibrium curve; instead, it moves short-relaxation charges toward the corresponding 60 min long-rest reference before recalculating ICA. Under strict cross-cell validation, the framework improves the comparability of the P2–P4 fingerprint windows within clear boundaries: 40% depth of discharge is a stable success region, 70% is condition-dependent, and 100% remains the most challenging scenario. A temperature-aware extension provides only localized additional benefit, mainly in the hardest cases. Overall, these results show that part of the apparent evolution of ICA fingerprints under practical testing can arise from relaxation-induced kinetic masking rather than irreversible material change, and highlight relaxation standardization as a protocol-aware route toward more reliable ICA fingerprint interpretation from cycler-accessible signals. The standardized fingerprints should therefore be interpreted as long-rest-referenced responses with improved comparability.

1 Introduction

Incremental capacity analysis (ICA) links galvanostatic voltage measurements to material-specific fingerprints in lithium-ion batteries[1]. In a battery cell, electrode phase transitions, lithiation and delithiation processes, local thermodynamic slopes, and polarization effects are all reflected in the measured terminal-voltage trajectory[2]. Upon differentiation, these features manifest as characteristic structures in the dQ/dU domain[3]. Consequently, ICA is frequently regarded as a form of electrochemical voltage spectroscopy, rather than solely a feature-extraction method for state-of-health estimation[4]. The mechanistic utility of ICA, however, relies on the voltage trajectory providing a consistent electrochemical projection across tests. The measured voltage encompasses not only material thermodynamics but also ohmic, kinetic, and transport-related overpotentials[5]. Variations in these non-equilibrium contributions, driven by test protocols or prior cell history, can alter IC fingerprints, even if the underlying material state remains unchanged[6].

This consideration is particularly significant for commercial layered-oxide/graphite cells, where the IC response represents a superposition of positive- and negative-electrode processes[7]. Graphite staging transitions, cathode phase changes, lithium redistribution, impedance growth, and variations in electrode utilization all influence the measured dQ/dU response[8–10]. Under well-controlled, low-rate, or extended-rest conditions, these fingerprints can facilitate the interpretation of degradation. In practical diagnostic scenarios, however, the voltage trajectory often includes a substantial non-equilibrium component[11]. Increases in current, changes in prior usage, or reduced relaxation time before charging can intensify residual polarization and concentration gradients. As a result, apparent changes in IC features should not be directly attributed to loss of lithium inventory, loss of active material, impedance growth, or phase-response evolution without accounting for protocol-induced components of the voltage response[12].

Numerous efforts to enhance the practicality of ICA have focused on extracting meaningful descriptors from non-ideal charging data, such as partial charging segments, varying charge initiation states, and different charging rates[13–15]. Recent studies have further advanced this direction toward minute-level ICA reconstruction from sparse charging segments, few-point electrode-level diagnosis, cloud-based IC-feature SOH estimation, and physics-informed, transferable degradation

[a] Energy Materials & Interfaces (EMI) Group, Department of Applied Physics, Aalto University, Espoo, 00076 Finland.
[b] Energy Technology, Technical University of Munich, Campus Straubing for Biotechnology and Sustainability, 94315 Straubing, Germany.
[c] Weihenstephan-Triesdorf University of Applied Sciences, 94315 Straubing, Germany.

† Footnotes relating to the title and/or authors should appear here.
Supplementary Information available: [details of any supplementary information available should be included here]. See DOI: 10.1039/x0xx00000x

View Article Online
DOI: 10.1039/D5TA03434A

modeling[16–19]. While these studies are valuable for engineering applications, they do not fully address a fundamental materials question: when the cell state and diagnostic charge conditions are otherwise constant, to what extent is observed IC variation attributable solely to the relaxation history preceding charge? Pre-charge relaxation is a critical procedural factor, as it determines the level of residual polarization and concentration imbalance present at the onset of the next diagnostic charge[20,21]. If this residual non-equilibrium state persists in the voltage trajectory, it can obscure the material-specific fingerprint that ICA aims to reveal[22].

This phenomenon is termed relaxation-induced kinetic masking. When relaxation is brief, the diagnostic charge arises from an altered electrochemical background that can persist during charging and modify the voltage profile of local electrode processes. After transformation into dQ/dU, even moderate voltage deviations may manifest as peak displacement, centroid drift, or area redistribution within an ICA fingerprint window[6]. Apparent peak evolution can thus result from protocol-induced masking. This issue is particularly significant when ICA descriptors are used to interpret degradation mechanisms, as interpretations related to loss of active material, loss of lithium inventory, impedance, or phase response may be confounded by recent relaxation history[23].

To isolate this effect, a controlled full-lifetime aging dataset comprising 12 commercial NMC-type 21700 cells was utilized. For each reference performance test, four ICA-related diagnostic charges were performed at identical charge rates and depth of discharge (DoD), with only the pre-charge relaxation duration varied among 60, 30, 10, and 0 minutes. The 60-minute case serves as a practical long-rest reference, while the shorter-rest cases demonstrate how insufficient relaxation distorts the voltage trajectory and the resulting IC fingerprints. By comparing within the same cell and at the same test checkpoint, relaxation-induced masking can be more effectively distinguished from variations in cell identity, aging trajectory, diagnostic current, or DoD.

The primary objective of this study is to establish relaxation-induced ICA distortion as a structured electrochemical projection. Both the voltage domain and the dQ/dU domain are analyzed using reproducible fingerprint windows P1–P4. These windows are not interpreted as strict single-phase assignments, but rather as experimentally reproducible voltage regions encompassing overlapping contributions from electrode phase responses, thermodynamic slope changes, polarization, and lithium redistribution. The secondary objective is to determine whether a portion of this kinetic masking can be mitigated prior to material-related interpretation. To this end, a voltage-domain relaxation lens is developed, based on an effective voltage bias descriptor, $\tau(U)$. This lens is applied to the voltage trajectory before ICA recalculation, as the distortion originates in the voltage response and is subsequently amplified in dQ/dU[24].

The results indicate that relaxation-induced masking is systematic, window-dependent, and condition-dependent. The $\tau(U)$-based relaxation lens can partially align short-rest IC fingerprints with the corresponding 60-minute long-rest reference, but only within defined boundaries. The 40% depth-of-discharge condition represents a stable region of success, 70% exhibits mixed outcomes, and 100% remains the most challenging regime. Descriptor-level analysis reveals that the correction is more effective for centroid- and area-related metrics than for fine peak-height geometry. These findings reinterpret short-relaxation ICA distortion as a protocol-induced contribution that can generate pseudo-evolution in material-related fingerprints. Therefore, accounting for this contribution is essential before using ICA to infer degradation mechanisms from cycler-accessible signals.

2 Controlled relaxation protocol for isolating kinetic masking

The dataset was constructed to isolate pre-charge relaxation history within otherwise matched ICA comparisons. Twelve commercial Samsung INR21700-50E cells, NMC-type 21700-format cells with a nominal capacity of 4.9 Ah, were aged under a common cycling protocol and characterized using a repeated reference performance test (RPT) template. All measurements used in this work were conducted at 25 °C. A total of 166 complete RPTs were available across the 12 cells; the cell-level aging coverage and diagnostic-condition matrix are provided in Table S1, ESI†. The central comparison in this work is not a cross-cell aging-trajectory comparison, but a within-RPT relaxation comparison: for each complete RPT, short-rest diagnostic charges are compared with the corresponding 60 min charge from the same cell, the same aging checkpoint, and the same diagnostic condition.

Fig. 1 summarizes the repeated RPT sequence. Each RPT included a capacity measurement, a low-rate C/25 reference charge, four ICA-related diagnostic charges, and current-interrupt tests. The four ICA-related charges form the controlled relaxation set used in this study. Within the same cell and RPT, these charges were conducted at identical diagnostic C-rate and DoD, while only the pre-charge relaxation duration was varied to 60, 30, 10, and 0 minutes. The 60 min case is used as the practical long-rest reference; the 30 and 10 min cases are the main short-rest standardization targets; and the 0 min case is retained primarily to characterize the extreme non-relaxed distortion. The 60 min duration was selected as a practical upper-bound relaxation period in the repeated RPT design: it provides a substantially relaxed diagnostic condition while keeping the total RPT duration compatible with repeated full-lifetime aging characterization. Longer rest periods could further reduce residual non-equilibrium contributions, but would substantially increase the time cost of each repeated diagnostic checkpoint. Therefore, the 60 min case is treated as a practical long-rest condition. Detailed charge-case definitions are provided in Table S2, ESI†.

To examine the condition dependence of relaxation-induced kinetic masking, the cells covered four diagnostic charge rates, 0.1, 0.3, 0.7, and 1.0 C, and three DoD levels, 40, 70, and 100%. Each cell retained one assigned diagnostic C-rate–DoD combination throughout aging. This design provides two levels

View Article Online
DOI: 10.1039/D5TA03434A

of information: within each complete RPT, the relaxation-duration effect can be isolated under a fixed cell state and diagnostic condition; across the available C-rate–DoD matrix, the dependence of RSI and standardization response on diagnostic condition can be evaluated. Since each C-rate–DoD combination was represented by one cell, the condition-resolved results are interpreted as structured trends across the available cell-condition matrix rather than as fully replicated factorial effects. The focused comparison in this study remains the within-RPT relaxation-duration comparison. The C/25 charge and current-interrupt measurements were used only as supporting measurements. The C/25 charge provides a low-polarization reference landscape but is not used as the standardization target, because doing so would mix relaxation effects with changes in current, polarization background, and charge path. The current-interrupt tests help contextualize local short-time polarization but are not direct inputs to the voltage-domain standardization framework.

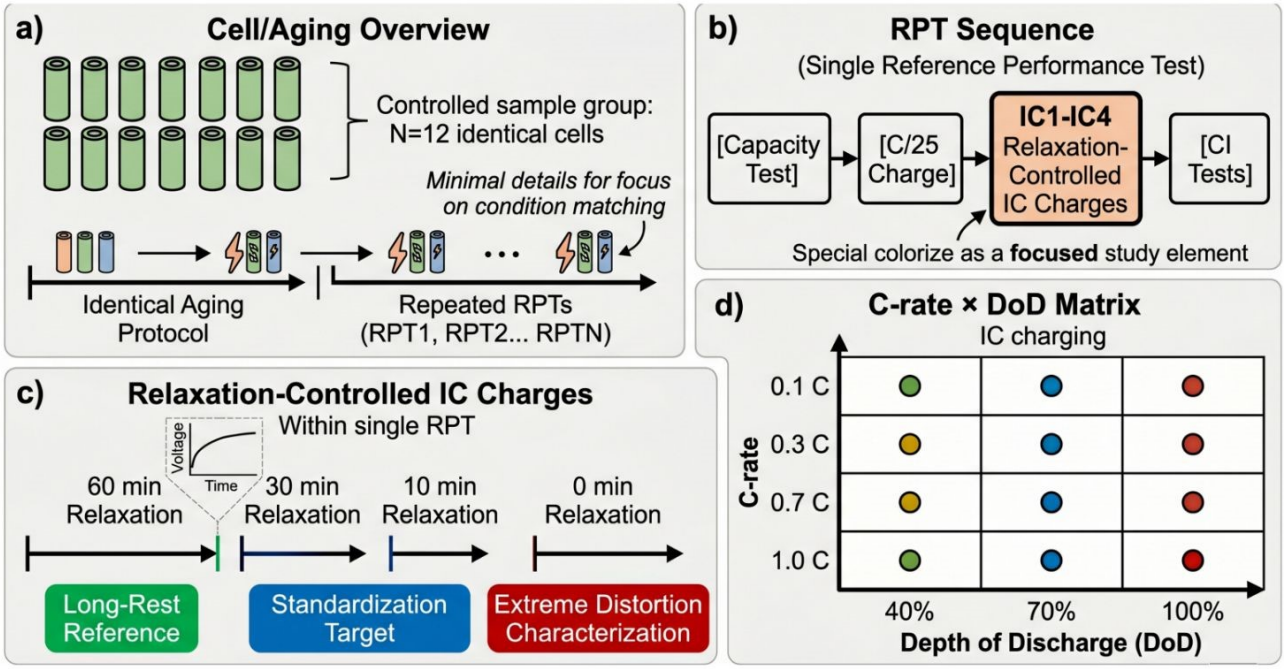

Fig. 1. Controlled relaxation protocol used to isolate relaxation-induced kinetic masking.

3 Relaxation-induced kinetic masking of ICA fingerprints

The controlled relaxation protocol allows the effect of insufficient pre-charge relaxation to be examined before any voltage standardization is applied. Fig. 2 shows a representative RPT in which the cell state, diagnostic C-rate, DoD, and test sequence are fixed, while only the pre-charge relaxation duration is changed. Four reproducible regions are identified in the long-rest IC response and denoted as P1–P4 (Fig. 2a). These regions are used as fingerprint windows, because the measured IC response contains overlapping contributions from positive- and negative-electrode phase responses, thermodynamic slope changes, lithium redistribution, and polarization[4]. This window-based definition avoids overassigning individual peaks while still enabling reproducible comparisons across relaxation duration, aging state, and diagnostic condition.

Changing only the pre-charge relaxation duration already produces a systematic difference in the charging-voltage trajectory (Fig. 2b). This voltage-domain difference appears moderate in the U–Q representation, but it becomes more pronounced after differentiation. The corresponding IC curves show peak displacement and intensity changes within the same fingerprint windows (Fig. 2c). This behavior reflects the differential nature of ICA: a protocol-induced voltage shift can be amplified in the dQ/dU domain, especially in voltage regions with plateau-like responses. The observed IC variation should therefore not be treated as a numerical artifact or a smoothing issue; it is the differential expression of a modified voltage projection.

The projection originates from the electrochemical background retained after short relaxation. Residual polarization and concentration imbalance from the previous state remain at the beginning of the subsequent diagnostic charge and continue to evolve during charging[25,26]. The resulting distortion is voltage-window-dependent, because ohmic, kinetic, and diffusion-related overpotentials vary with current, the voltage region, and the local electrode state. In graphite-based LIBs, this state dependence is further strengthened by SOC-dependent lithium redistribution and equilibration kinetics[27]. The same material state can therefore be projected onto different voltage trajectories depending on the relaxation history.

View Article Online DOI: 10.1039/D6TA03434A

From a material interpretation perspective, this behavior constitutes relaxation-induced kinetic masking. The material-related fingerprint remains present, but it is observed through an additional non-equilibrium layer introduced by the test protocol. A fingerprint window may shift, change its local center, or redistribute its area because of residual relaxation history. This distinction is essential when ICA descriptors are used to discuss degradation-related chemistry: without accounting for relaxation history, protocol-induced changes may be overassigned to LAM-, LLI-, impedance-, or phase-response-related evolution.

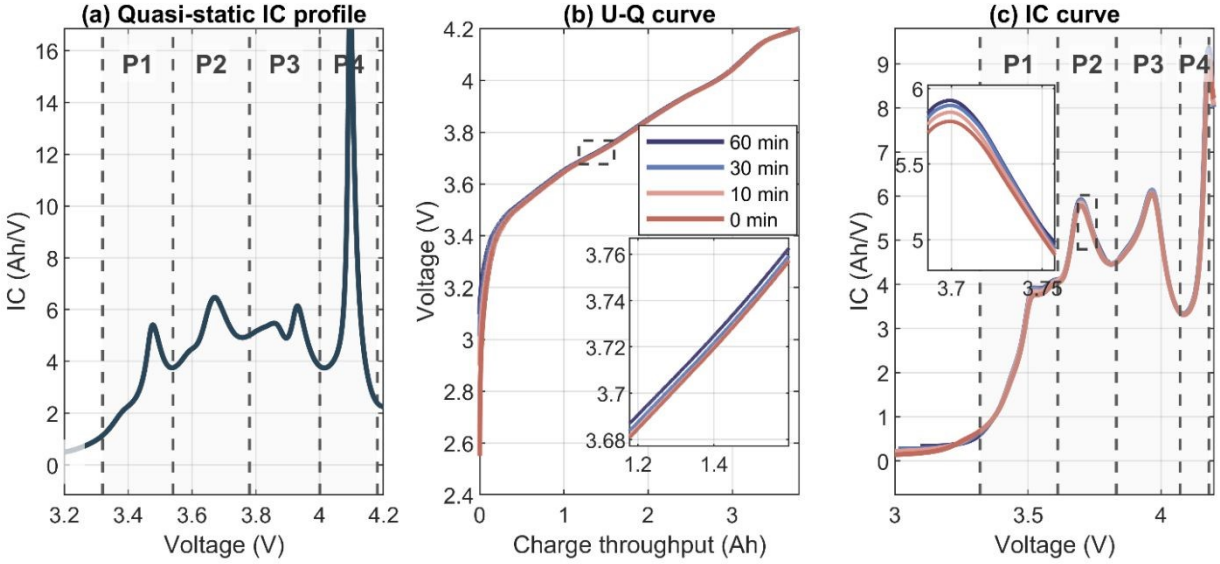

Fig. 2. Representative relaxation-induced distortion in voltage and IC domains. (a) Long-rest IC response with the reproducible fingerprint windows P1–P4. (b) Voltage trajectories under different pre-charge relaxation durations within the same RPT. (c) Corresponding IC curves showing relaxation-dependent peak displacement and intensity variation.

To quantify this effect across the full dataset, we employed a relaxation sensitivity index (RSI), defined in Section S2 of the ESI†. The global RSI measures the deviation of a short-rest IC curve from the corresponding 60 min reference, whereas the window RSI evaluates this deviation within a predefined fingerprint window. As shown in Fig. 3a, the global distortion decreases with increasing relaxation duration. Across all 166 RPTs, the median global RSI decreases from 7.87% at 0 min to 5.92% at 10 min and 3.62% at 30 min. This monotonic trend indicates that short relaxation introduces a structured protocol-dependent contribution.

Global RSI alone, however, does not fully describe the masking effect. Fig. 3b shows that DoD determines which fingerprint windows are sampled during the diagnostic charge. P4 is covered across all DoD levels, whereas P3 is only partially covered at 40% DoD, P2 is nearly absent at 40% DoD and only partly covered at 70% DoD, and P1 is fully accessible only at 100% DoD. Thus, DoD affects not only the magnitude of the measured distortion, but also the observable part of the fingerprint. Full C-rate × DoD distortion maps for the 30, 10, and 0 min cases are provided in Fig. S1, ESI†.

The local descriptors further show that relaxation-induced masking is not uniformly distributed across the voltage range. Fig. 3c–e summarize representative 10 min window-level results, while the complete window-RSI maps and SOH-correlation analysis are provided in Figs. S2 and S3, ESI†. In many cases, the distortion appears not as a simple peak-height change, but as a shift in the local response center and a redistribution of the response area within a fingerprint window. For example, P3 at 40% DoD shows a median centroid shift of approximately 7.36 mV and a relative AUC distortion of 8.27%. For P2 at 70% DoD, the corresponding values are approximately 8.98 mV and 12.79%. These descriptors are less dependent on robust single-peak detection and better capture how a local fingerprint is displaced or reweighted by relaxation history.

The dependence on SOH is also condition-specific. The window RSI does not follow a single monotonic trend with aging across all DoD–window combinations, indicating that aging modifies the sensitivity of local voltage regions to insufficient relaxation in a window- and condition-dependent manner. In this study, SOH is therefore treated as a stratifying dimension together with charge rate, DoD, and fingerprint-window location.

Overall, Fig. 2 and Fig. 3 establish insufficient pre-charge relaxation as a structured kinetic masking effect in ICA. The masking originates in the voltage trajectory, is amplified in the differential domain, and appears as peak displacement, centroid drift, and area redistribution within material-related fingerprint windows. These findings motivate a voltage-domain standardization strategy: before ICA fingerprints are interpreted as material-related signatures, the short-rest voltage trajectory should first be referenced to the corresponding long-rest condition.

View Article Online
DOI: 10.1039/D6TA03424A

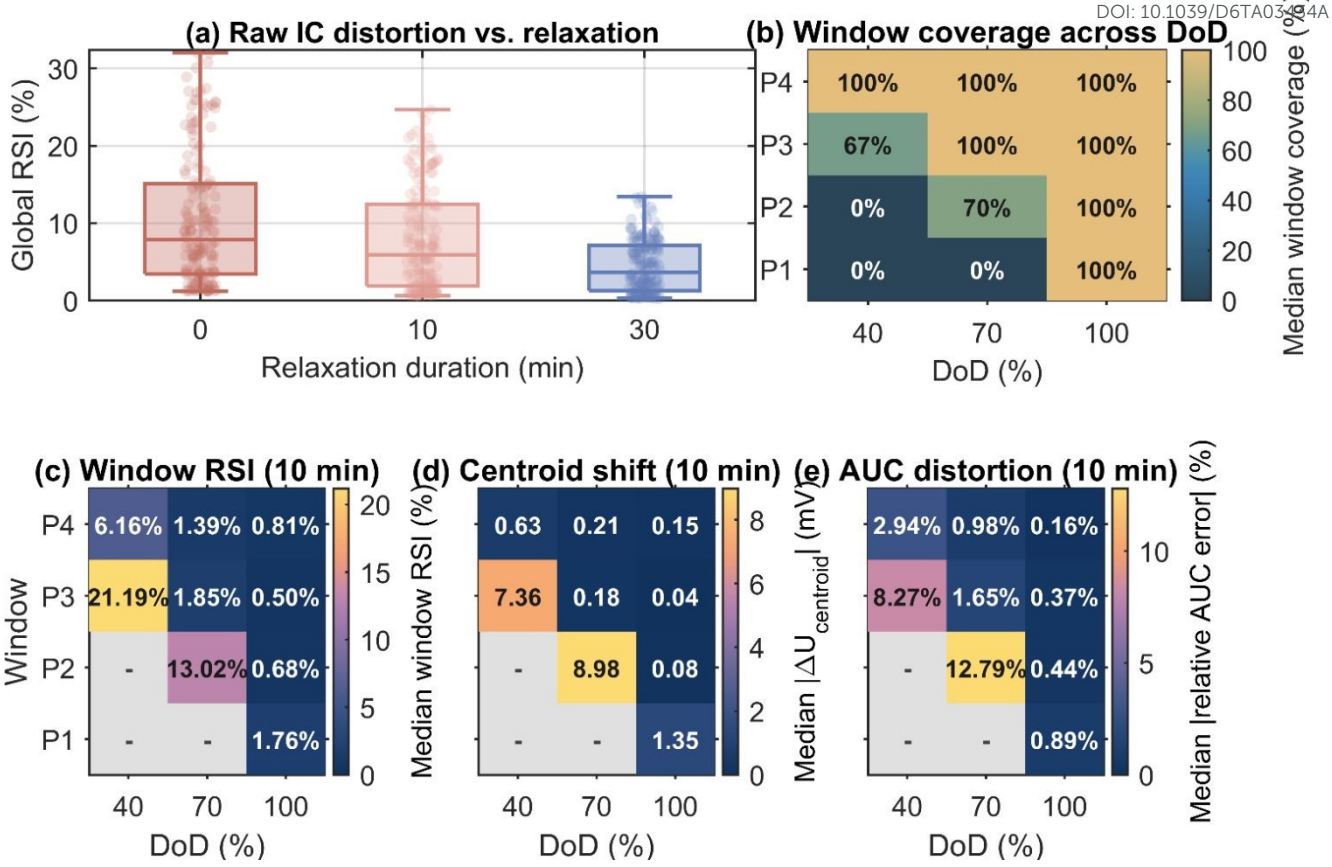

Fig. 3. Characterization of relaxation-induced kinetic masking. (a) Global RSI distributions for the 30, 10, and 0 min relaxation cases relative to the 60 min reference. (b) Operational coverage of P1–P4 under different DoD conditions. (c) Representative 10 min window-level RSI map. (d) Median centroid shift and (e) relative AUC distortion for representative window-level comparisons.

4 Voltage-dependent relaxation lens for fingerprint standardization

The results in Section 3 show that relaxation-induced masking originates in the charging-voltage trajectory and is then amplified in the differential IC representation. For this reason, the standardization is applied before differentiation. Instead of empirically correcting the IC curve after it has been calculated, the short-rest voltage trajectory is first referenced to the corresponding long-rest trajectory under the same diagnostic condition. ICA is then recalculated from the standardized voltage curve. This sequence follows the physical order of the distortion: insufficient relaxation changes the electrochemical background at the beginning of charge, this background propagates through the measured voltage trajectory, and the resulting voltage deviation appears as an apparent fingerprint change in dQ/dU.

The 60 min relaxation charge is used as the practical long-rest reference for each RPT. This reference is not assumed to represent an ideal equilibrium state[28]; rather, it preserves the controlled-variable logic of the experiment by sharing the same diagnostic C-rate and DoD as the short-rest charges. Within the available relaxation-controlled sequence, it is the longest and most relaxed diagnostic charge measured under otherwise identical conditions. It was therefore selected as the internal reference for RSI calculation and voltage-domain standardization. The 30 and 10 min relaxation charges are treated as the primary standardization targets, whereas the 0 min case is retained primarily for distortion characterization. The subsequent evaluation focuses on the P2–P4 fingerprint windows, because P1 is more sensitive to low-voltage boundary effects and incomplete coverage.

The framework is built around τ(U), which is defined here as a compact effective descriptor of the transferable relaxation-induced voltage bias in the voltage domain. This quantity is not interpreted as a unique microscopic time constant of a single electrode process[29]. Instead, it is used as a compact descriptor of how the transferable part of the relaxation-induced voltage offset decays across voltage regions[30]. This restrained interpretation is important because the terminal voltage of a commercial battery contains overlapping contributions from electrode thermodynamics, charge-transfer kinetics, ohmic resistance, concentration polarization, and lithium redistribution[8]. The role of τ(U) is therefore not to separate these processes, but to provide a voltage-domain lens for attenuating the dominant short-rest masking contribution using only cycler-accessible signals.

The construction of τ(U) follows the controlled relaxation design. Within each RPT, charges with different relaxation durations are aligned and compared with the 60 min reference to estimate how the voltage offset depends on relaxation time

and voltage region. The resulting fitted τ-function is mapped to the voltage domain so that it can be applied along the measured charging trajectory. To improve cross-cell transferability, the implementation combines a global relaxation function with a C-rate-stratified function through a shrinkage strategy. This retains the observed rate dependence of relaxation-induced masking while reducing overfitting to sparse condition-specific data. Details of charge-progress alignment, τ(U) identification, voltage-domain mapping, cell-level aggregation, and shrinkage are provided in Section S4 of the ESI†.

For each short-rest charge, the immediately preceding relaxation segment is employed to estimate the residual non-equilibrium contribution retained at the beginning of the diagnostic charge. This contribution is then propagated along the subsequent charging trajectory using τ(U), giving a voltage-domain offset that is subtracted from the measured short-rest voltage. The standardized voltage trajectory is then interpolated onto the common voltage grid, and ICA is recalculated using the same processing workflow as for the raw fingerprints. Low-voltage region gating and amplitude clipping are applied as stabilization constraints to reduce overcorrection near boundary-sensitive regions and to keep the propagated correction within the range supported by the measured relaxation signal; their implementation is described in Section S4 of the ESI†.

The workflow is summarized in Fig. 4. In this study, the τ(U)-based framework is best viewed as a voltage-domain relaxation lens. It estimates and attenuates the transferable component of the short-rest kinetic masking layer before differentiation, thereby recalculating the IC fingerprint on a more comparable long-rest-referenced voltage background. The model does not claim to recover an equilibrium voltage curve or to identify microscopic relaxation processes. Its purpose is to test whether part of the apparent ICA fingerprint evolution is a removable protocol-induced contribution. The success and failure patterns of this lens are examined in the next section.

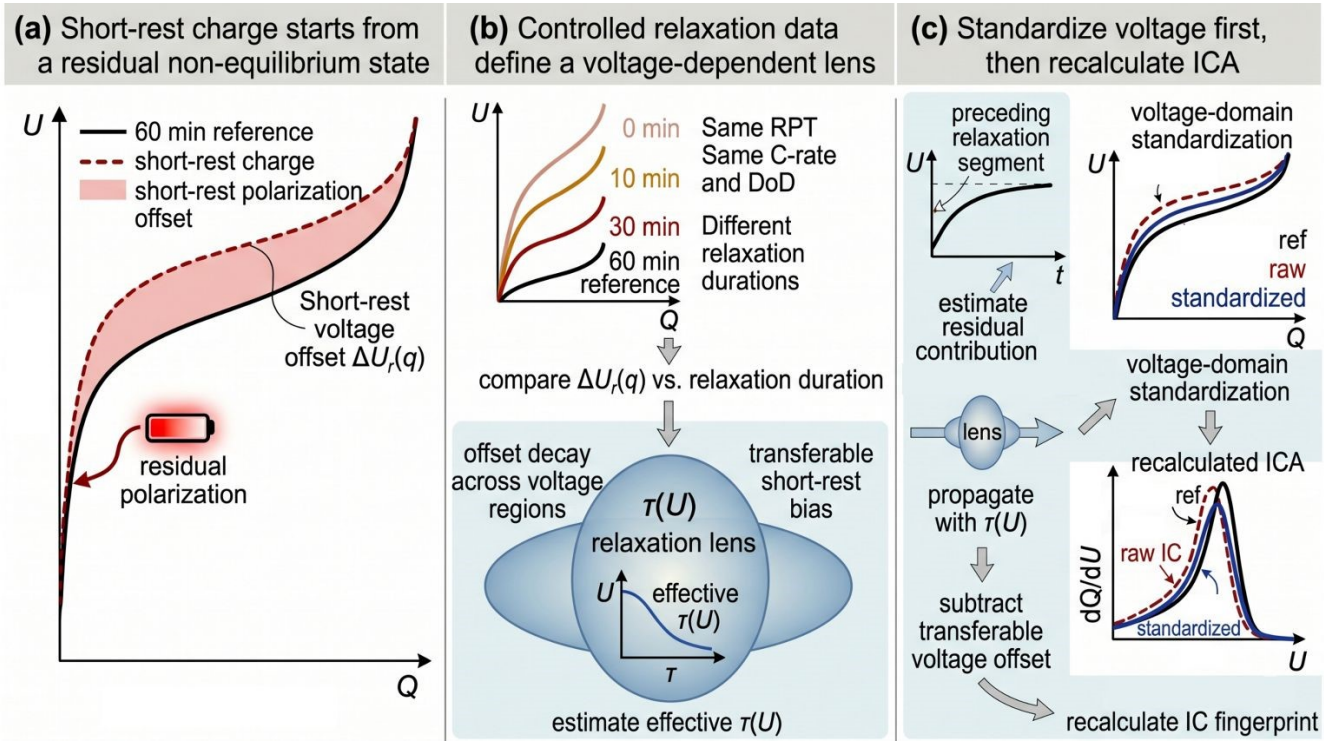

Fig. 4. Voltage-domain relaxation lens for ICA standardization: Workflow of the τ(U)-based framework.

5 Restored comparability and correctability boundary

Having established that short relaxation creates a structured kinetic masking layer, we examine whether the τ(U)-based relaxation lens can attenuate a transferable part of this layer under cross-cell validation. The target is to test whether material-related fingerprint windows can be moved toward a more comparable 60 min-referenced voltage background. A positive gain, therefore, indicates reduced protocol-induced masking. In contrast, condition-dependent or negative gains define regimes in which relaxation history is too distributed for the present first-order voltage-domain lens.

Fig. 5 summarizes the baseline standardization results in the P2–P4 fingerprint windows. For each test cell, all model parameters are estimated from the remaining cells using the leave-one-cell-out protocol described in Section S4 of the ESI†. Across the target cases, the standardized fingerprints shift toward the positive-gain side (Fig. 5a), indicating that short-rest distortion contains a transferable component. For the 30 min cases, the mean and median reductions in P2–P4 RSI are 0.59% and 0.45%, respectively. For the 10 min cases, the corresponding values are 0.51% and 0.44%. Full statistics, including positive-improvement fractions and Wilcoxon signed-rank test results, are provided in Table S3, ESI†.

View Article Online
DOI: 10.1039/D6TA03434A

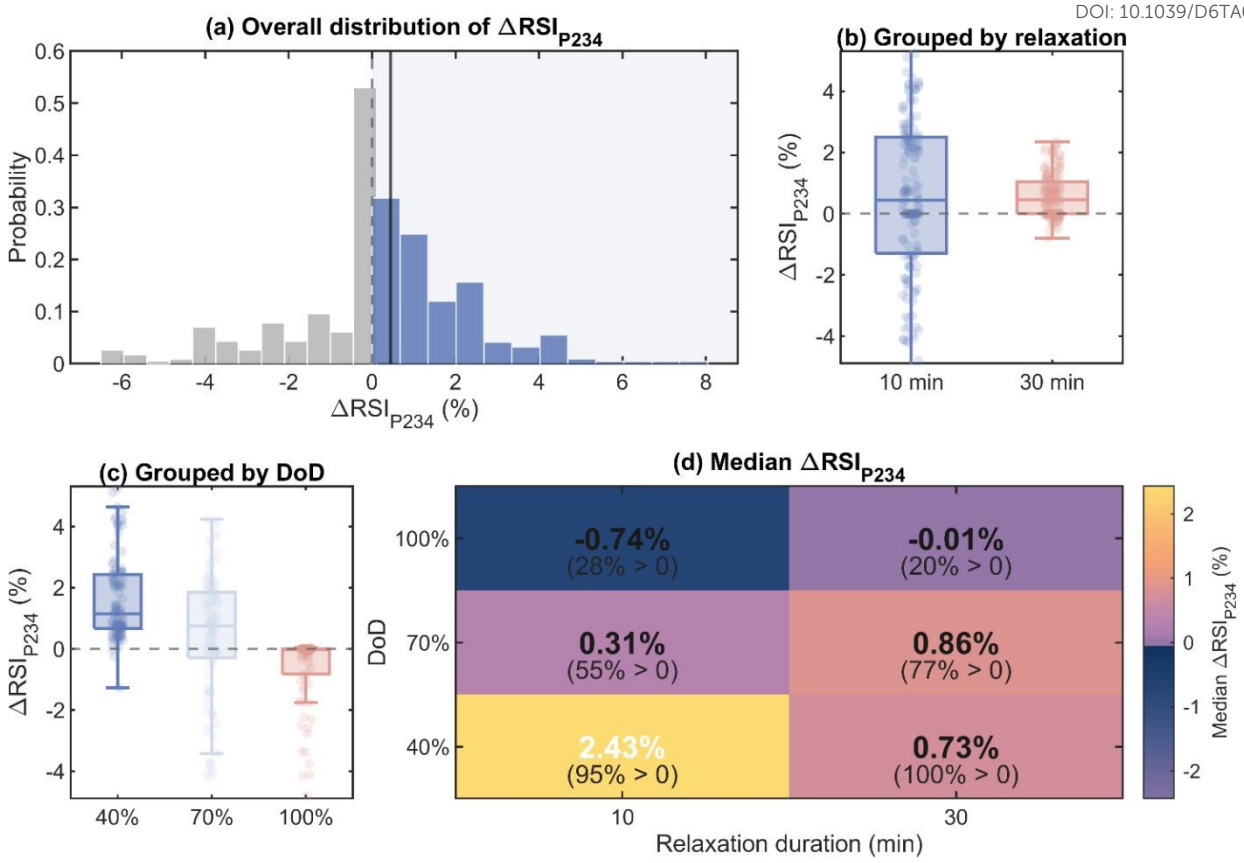

Fig. 5. Cross-cell validation of the baseline τ(U) relaxation lens. (a) Case-wise P2–P4 RSI reduction after standardization. (b) Comparison between 30 and 10 min cases. (c,d) DoD-stratified standardization performance.

The comparison between 30 and 10 min relaxation reflects the expected difficulty of the standardization task (Fig. 5b). The 30 min case is closer to the 60 min reference and requires a smaller extrapolation of the residual voltage contribution. The 10 min case starts from a stronger non-equilibrium background, so the propagated correction is larger and less certain. Nevertheless, both subsets show positive median gain, supporting the interpretation that the short-rest bias contains a first-order component that can be transferred across cells.

Within the available cell-condition matrix, the more informative boundary is set by DoD (Fig. 5c,d). At 40% DoD, the baseline lens shows stable improvement, with mean and median P2–P4 RSI reductions of 1.70% and 1.14%, and a positive-improvement fraction of 97.6%. At 70% DoD, the response becomes condition-dependent, with mean and median reductions of 0.48% and 0.74%. At 100% DoD, the limitation becomes clear: the mean gain is negative, the median remains close to zero, and only 24.0% of cases improve. These results define a three-level correctability boundary: 40% DoD is a stable success region, 70% DoD is a mixed region, and 100% DoD is the hardest scenario. DoD-stratified statistics are summarized in Table S4, ESI†.

This boundary is not only a statistical partition. It reflects the distribution of relaxation-induced masking along the diagnostic charge path. At shallow or moderate DoD, the short-rest bias is sampled over a more limited portion of the voltage trajectory and is more often approximated as a removable voltage-domain contribution. At 100% DoD, however, the diagnostic charge starts from a deeper low-SOC state and spans the full operational voltage range. The preceding deep-discharge preparation can leave a more spatially and electrochemically distributed non-equilibrium background, including steep residual solid-phase concentration gradients, electrolyte concentration imbalance, and local overpotential components that depend on electrode stoichiometry. During the subsequent charge, these contributions do not simply decay as a single voltage-domain offset. Instead, they can be redistributed as the cell traverses different graphite staging regions and positive-electrode response regions. The resulting relaxation memory is therefore path-coupled and multi-timescale: the apparent voltage bias at a given voltage is affected not only by the local value of U, but also by the preceding SOC range and by the evolution of residual concentration gradients along the charge path. This behavior violates the central simplification of the baseline lens: that the dominant short-rest contribution can be treated as a transferable voltage-domain bias whose decay is mainly parameterized by the present voltage. In the deep-DoD case, the observed voltage bias is more likely a superposition of several residual contributions with different spatial origins and relaxation rates, including particle-scale diffusion imbalance,

View Article Online
DOI: 10.1039/D5TA03434F

electrolyte redistribution, and state-dependent interfacial polarization. A single τ(U)-based descriptor can therefore attenuate only the transferable first-order component, and cannot fully represent this distributed path memory. Complete condition-resolved maps across diagnostic C-rate and DoD are provided in Fig. S4, ESI†.

The descriptor-level results clarify what type of fingerprint comparability is restored (Fig. S5, ESI†). The gain is window-dependent. P2 is the most sensitive window when sufficiently covered, while improvements in P3 and P4 are more concentrated at 40% DoD. The relaxation lens preferentially improves position- and area-related descriptors. For P2 at 70% DoD, the median reduction in centroid-error magnitude is approximately 3.18 mV, and the corresponding reduction in relative AUC error is approximately 3.92%. In contrast, peak-height errors show solely limited improvement. This distinction is central to the interpretation of the framework: the voltage-domain lens primarily reduces protocol-induced displacement and area redistribution, but it does not fully reconstruct the fine-peak-height geometry.

Representative curve-level examples are shown in Fig. 6. In the easy case, the standardized voltage trajectory and recalculated IC fingerprint move closer to the 60 min reference (Fig. 6a,d). In the split case, the voltage-domain correction improves part of the local fingerprint while leaving other regions less affected (Fig. 6b,e). In the hard case, the relevant deviation is not effectively reduced, and the standardized IC curve remains poorly aligned with the reference (Fig. 6c,f). These examples make the correctability boundary visible at the curve level: the relaxation lens is effective when the short-rest distortion behaves as a transferable voltage-domain masking layer, but it fails when path history and accumulated non-equilibrium contributions become too distributed or window-coupled.

Together, Figs. 5–6 indicate that the proposed standardization restores fingerprint comparability in a limited but mechanistically interpretable manner. The success cases demonstrate that part of the apparent short-rest fingerprint evolution is protocol-induced and can be attenuated using cycler-accessible voltage signals. The failure cases are equally informative: they mark regimes where a single τ(U)-based lens is insufficient and where additional state variables, multi-timescale relaxation, or more targeted experimental separation may be required.

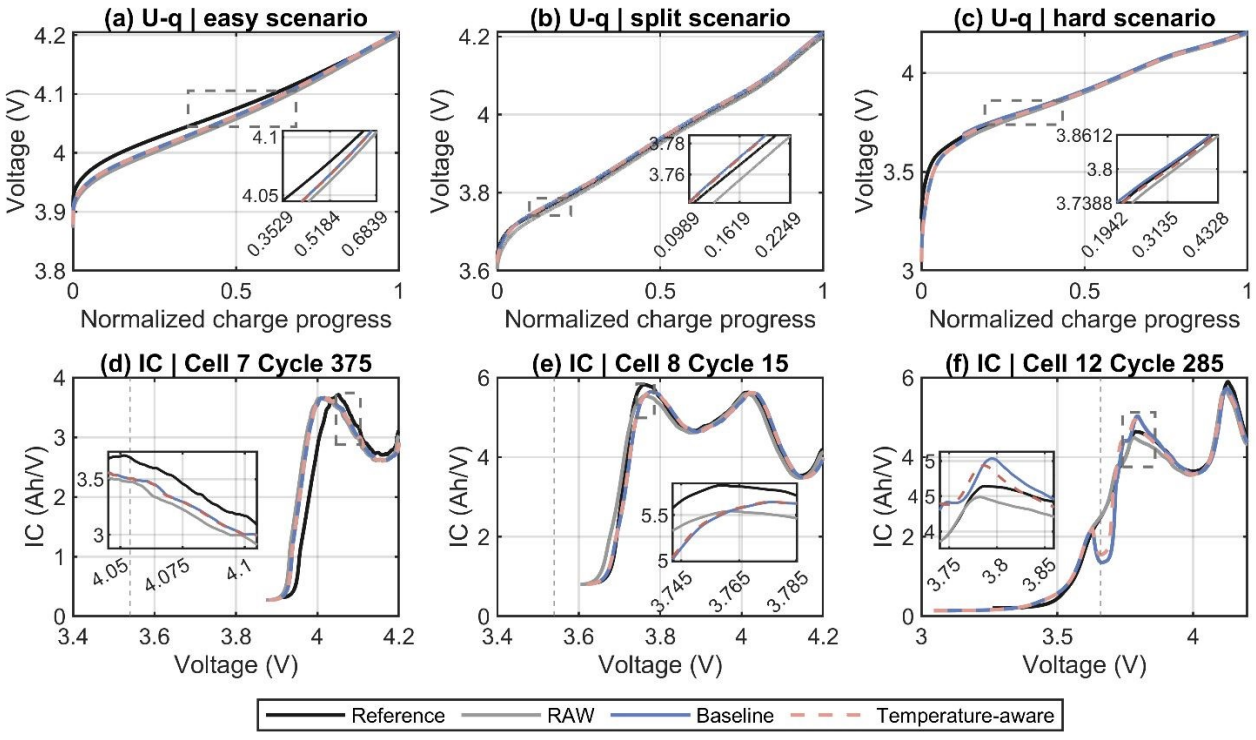

Fig. 6. Representative curve-level standardization examples. (a–c) Voltage trajectories and (d–f) recalculated IC fingerprints for easy, split, and hard scenarios.

6 Temperature-history contribution as a probing extension

The baseline τ(U) relaxation lens captures a transferable first-order component of the short-rest voltage bias, but the residual errors in the hardest cases suggest that not all state-history effects are represented by voltage-dependent relaxation alone. Thermal history is one possible contributor because temperature can modify polarization decay and relaxation kinetics during both the pre-charge rest and the subsequent diagnostic charge[31]. To examine this possibility, we introduced

View Article Online
DOI: 10.1039/D5TA07134H

a temperature-aware extension as a mechanistic probe. In this extension, temperature is not treated as an independent voltage-offset term. Instead, it modifies the local τ(U,T) value used in the effective voltage-bias propagation, thereby altering the decay of the residual polarization contribution. The full formulation, including the temperature-dependent τ(U,T) parameter, reference-temperature trajectory, and reconstruction procedure, is provided in Section S6 of the ESI†.

The temperature-aware extension remains close to the baseline trend and provides only localized additional benefit. At the subset level, it does not introduce a fundamentally different correction pattern. The clearest improvement appears in the hardest regime. In the 100% DoD cases, the mean P2–P4 RSI reduction increases from −0.82% for the baseline model to −0.38%, and the positive-improvement fraction increases from 24.0% to 34.0%. The strongest incremental gain occurs in the 100% DoD / 10 min subset, whereas most other conditions show incremental gains close to zero or slightly negative. Complete statistics and case-wise comparisons are provided in Table S5 and Fig. S6, ESI†.

These results support a restrained interpretation. Thermal-history coupling may contribute to residual distortion when the charge path is deep, and the relaxation duration is short, but it cannot yet be compressed into a robust, globally beneficial correction term under the present data structure. The baseline τ(U) lens therefore remains the main framework for this study. The temperature-aware extension is interpreted as evidence that the hardest cases involve additional state-history variables beyond the dominant voltage-dependent relaxation component, including thermal history, path history, local state dependence, and multi-timescale relaxation.

7 Mechanistic implications for protocol-aware ICA interpretation

The results above demonstrate that ICA fingerprints are material-related, but not protocol-independent. An IC curve is often interpreted as a fingerprint of electrode phase responses, local thermodynamic slopes, lithium redistribution, and polarization[32,33]. However, this fingerprint is always measured through a specific electrochemical protocol. When the pre-charge relaxation history changes, the electrochemical background at the start of charge changes accordingly. The voltage trajectory is therefore modified before the IC curve is calculated, and part of the apparent fingerprint evolution can arise from protocol-induced non-equilibrium projection rather than irreversible material evolution.

This distinction is important because common ICA descriptors are often used as indicators of degradation modes. Peak displacement, local area changes, and peak-intensity variation may be associated with loss of lithium inventory, loss of active material, impedance growth, or changes in electrode utilization[7,34]. The present results show that the same types of descriptor changes can also be produced by insufficient relaxation alone. Short relaxation retains residual polarization, concentration imbalance, and path memory from the previous state; during the subsequent diagnostic charge, this retained history is projected onto the terminal voltage and amplified in the differential domain. A fingerprint window may therefore shift, broaden, or redistribute its area even when the underlying material state has not changed.

The value of the τ(U)-based standardization is to attenuate this transferable kinetic masking layer before ICA is recalculated. Its role should not be judged only by the absolute reduction in curve error. More importantly, it reduces protocol-induced displacement, centroid drift, and area redistribution within reproducible fingerprint windows. This explains why centroid- and AUC-related descriptors are more effectively restored than peak-height geometry. The framework therefore provides a more comparable long-rest-referenced voltage background for evaluating whether changes in a local fingerprint window are more likely to reflect material-related evolution or relaxation-history variation.

The correctability boundary also carries mechanistic information. In the deep-DoD scenario, especially at 100% DoD, the diagnostic charge spans a broader voltage range and crosses more fingerprint windows. Because the charge starts from a deeper low-SOC state, the retained relaxation history can include more distributed solid-phase concentration gradients, electrolyte imbalance, and local overpotential components inherited from the preceding discharge or rest sequence. Residual non-equilibrium contributions can then propagate, accumulate, and redistribute along the charge path. Under such conditions, short-rest distortion is less likely to be represented by a single first-order voltage-domain bias. Instead, additional state-history variables may be needed to describe how the residual non-equilibrium state evolves across voltage windows. The localized benefit of the temperature-aware extension further suggests that thermal history may contribute to the hardest cases, but that it is entangled with path history, local state dependence, and multi-timescale relaxation. Thus, failure cases do not simply indicate insufficient fitting; they identify scenarios in which additional state-history variables may need to be considered.

This interpretation also defines what the proposed framework does not claim. The standardized IC curve should not be regarded as a true thermodynamic ground-state fingerprint. It remains a protocol-dependent response measured under practical diagnostic conditions. The standardized curve is closer to the corresponding 60 min long-rest reference and therefore improves the comparability of material-related fingerprints. Similarly, the framework reduces the risk of overassigning relaxation-induced IC changes to LAM-, LLI-, impedance-, or phase-response-related degradation modes, but it does not independently identify real LAM, LLI, or specific structural transformations. Such assignments would require additional electrode-level or materials characterization, such as half-cell reconstruction, differential-voltage analysis with electrode support, operando measurements, or post-mortem characterization[35].

View Article Online
DOI: 10.1039/D6TA03434A

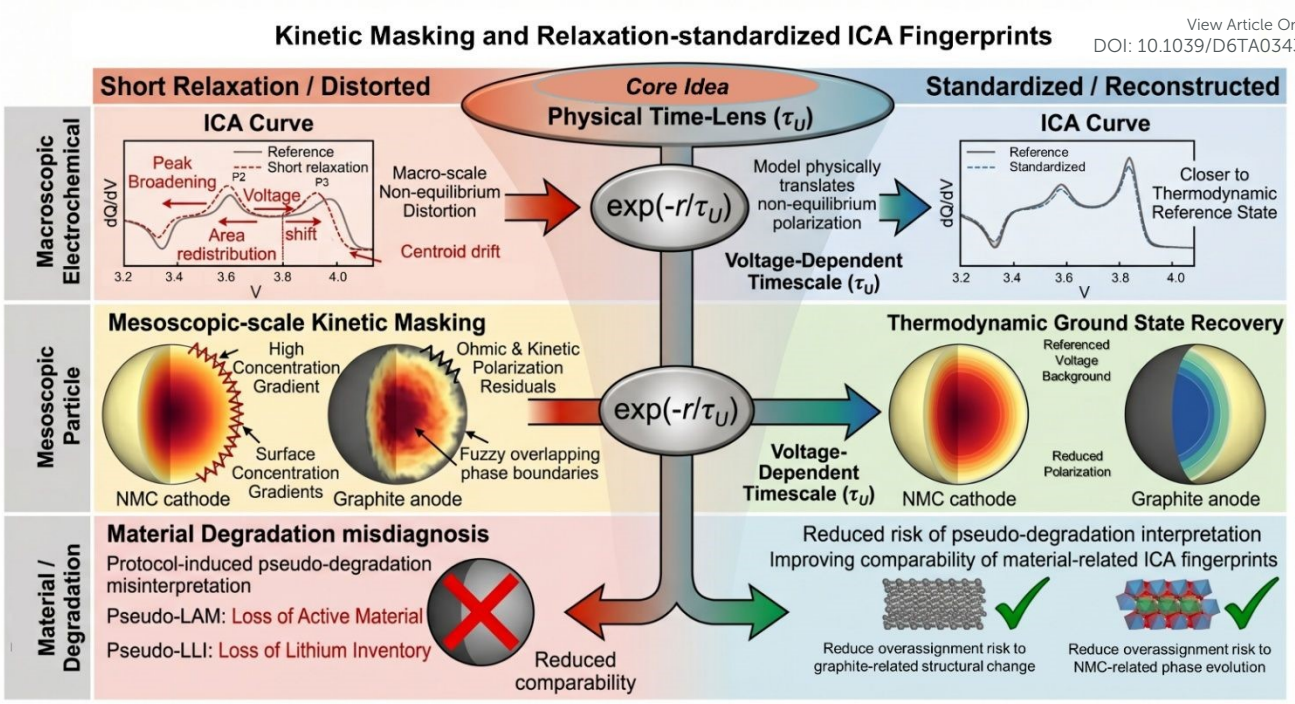

Fig. 7. Mechanistic description of protocol-aware ICA interpretation

The present validation was performed on commercial NMC/graphite batteries, and the τ(U)-based lens should therefore be regarded as a chemistry- and protocol-calibrated framework. In flatter voltage-plateau systems, such as $LiFePO_4$-based cells, relaxation-induced kinetic masking may be even more pronounced in the IC domain, because a small residual voltage bias can be strongly amplified when transformed into dQ/dU. In such systems, a short-rest relaxation history may therefore produce a larger redistribution of peak area for the same magnitude of voltage-domain deviation. Extending the present τ(U) framework to LFP cells may be more challenging, as two-phase plateau behavior can make the residual non-equilibrium state less compressible into a single descriptor. Similar caution applies to cells using Si-containing negative electrodes, where hysteresis and stress-coupled lithiation may introduce additional state variables. Therefore, the proposed framework is expected to remain conceptually useful as a protocol-aware standardization strategy, but τ(U) would need to be re-identified, and its correctability boundary revalidated for each material system and diagnostic protocol.

The mechanistic picture is summarized in Fig. 7. Under short relaxation, residual polarization, concentration imbalance, and path memory create a kinetic masking layer that distorts the voltage trajectory and the resulting ICA fingerprint. At the materials level, this retained non-equilibrium state can be understood as the cell manifestation of incomplete relaxation of concentration and chemical-potential gradients within active-material particles and the electrolyte phase, together with ohmic and interfacial polarization. These microscopic and mesoscopic relaxation processes are not directly observed in the present experiment; instead, they appear as a macroscopic voltage-relaxation signature accessible from the cycler. The voltage-dependent relaxation lens uses this cycler-accessible voltage signature as a physical-time-lens analogy, mapping the residual relaxation history onto an effective voltage-domain correction before recalculating the IC curve. In this sense, τ(U) acts as an effective descriptor of the transferable voltage-domain footprint of residual concentration-gradient relaxation and polarization decay. The standardized response is therefore not an equilibrium material fingerprint, but a long-rest-referenced fingerprint with improved comparability. This provides a protocol-aware route to reduce the interpretation of pseudo-degradation while preserving the material relevance of ICA under realistic diagnostic constraints.

8 Conclusion

Insufficient relaxation introduces a relaxation-induced kinetic masking layer into incremental capacity fingerprints. Analysis of a dataset with repeated charges after 60, 30, 10, and 0-minute relaxation within the same RPTs enabled isolation of relaxation history from aging path, C-rate, and DoD. Short relaxation periods initially alter the charging-voltage trajectory and subsequently amplify this deviation in the differential ICA domain, resulting in peak displacement, centroid drift, and area redistribution within reproducible fingerprint windows. These changes are determined by relaxation duration, diagnostic condition, and voltage window, suggesting that they result from protocol-induced non-equilibrium projection.

To reduce this masking prior to material-related interpretation, a voltage-domain relaxation lens was developed based on a compact effective descriptor of the transferable relaxation-induced voltage bias in the voltage domain, τ(U). This framework aligns practical short-rest charges with their

corresponding long-rest references under identical diagnostic conditions, then recalculates the ICA on a more comparable voltage background. Cross-cell validation demonstrates that this long-rest-referenced standardization improves comparability in the P2–P4 windows, but only within defined boundaries: 40% DoD is a stable success region, 70% DoD is condition-dependent, and 100% DoD represents the primary limit of correctability.

Descriptor-level results clarify the specific aspects restored by this standardization. The τ(U) lens reduces centroid- and AUC-related errors more effectively than peak-height errors, indicating that its primary contribution is attenuation of protocol-induced displacement and area redistribution. This approach decreases the risk of misattributing relaxation-induced pseudo-evolution to LAM, LLI, impedance, or phase-response-related material evolution. However, standardized ICA fingerprints cannot independently identify these irreversible mechanisms and should not substitute for electrode-level or materials characterization. The temperature-aware extension further indicates that thermal history may contribute to the most challenging cases, particularly at 100% DoD and 10-minute relaxation, but its benefit remains localized and cannot currently be represented as a robust global correction term.

Because the present validation is limited to commercial NMC/graphite batteries, extension to other material systems should be treated as a chemistry- and protocol-specific recalibration problem. Flatter-plateau systems such as $LiFePO_4$ may amplify small residual voltage deviations in the dQ/dU domain, whereas two-phase behavior may introduce additional path-dependent state variables. Future use of the framework should therefore re-identify τ(U) and revalidate the correctability boundary for each cell chemistry and diagnostic protocol.

In summary, the findings demonstrate that the testing protocol must be considered an integral component of measurement when ICA is used for degradation interpretation. Long-rest and short-rest IC curves should not be compared as if they originate from the same electrochemical background. A portion of the observed ICA-fingerprint evolution during practical testing arises from relaxation-induced kinetic masking and can be partially attenuated using only cycler-accessible signals. The remaining failure cases highlight situations where path history, thermal history, and multi-timescale relaxation exceed the corrective capacity of a single τ(U)-based lens. Future research should focus on experimental designs and models that explicitly separate these state-history effects. The present framework establishes a protocol-aware approach for more reliable comparison of material-related ICA fingerprints under realistic diagnostic constraints.

Acknowledgements

AI-assisted tools were used for language polishing and for improving the visual presentation of selected figures. All scientific content, data analysis, interpretation, and final manuscript preparation were performed and verified by the authors.

View Article Online
DOI: 10.1039/D6TA03434A

Y.X. acknowledges funding from the Research Council of Finland (RCF) Academy Research Fellowship – PULSE project (funding decision No. 371636) and the Technology Industries of Finland Centennial Foundation's Future Makers grant – FAST (Grant No. 5174).

References

1 E. J. McShane, P. P. Paul, T. R. Tanim, C. Cao, H.-G. Steinrück, V. Thampy, S. E. Trask, A. R. Dunlop, A. N. Jansen, E. J. Dufek, M. F. Toney, J. N. Weker and B. D. McCloskey, Multimodal quantification of degradation pathways during extreme fast charging of lithium-ion batteries, *J. Mater. Chem. A*, 2022, **10**, 23927–23939.

2 M. Dubarry and D. Anseán, Best practices for incremental capacity analysis, *Front. Energy Res.*, 2022, **10**. DOI: 10.3389/fenrg.2022.1023555.

3 J. Z. Olson, C. M. López and E. J. F. Dickinson, Differential Analysis of Galvanostatic Cycle Data from Li-Ion Batteries: Interpretative Insights and Graphical Heuristics, *Chem. Mater.*, 2023, **35**, 1487–1513.

4 L. Spitthoff, P. J. Vie, M. S. Wahl, J. Wind and O. S. Burheim, Incremental capacity analysis (dQ/dV) as a tool for analysing the effect of ambient temperature and mechanical clamping on degradation, *Journal of Electroanalytical Chemistry*, 2023, **944**, 117627.

5 F. Brosa Planella, W. Ai, A. M. Boyce, A. Ghosh, I. Korotkin, S. Sahu, V. Sulzer, R. Timms, T. G. Tranter, M. Zyskin, S. J. Cooper, J. S. Edge, J. M. Foster, M. Marinescu, B. Wu and G. Richardson, A continuum of physics-based lithium-ion battery models reviewed, *Prog. Energy*, 2022, **4**, 42003.

6 A. Fly and R. Chen, Rate dependency of incremental capacity analysis (dQ/dV) as a diagnostic tool for lithium-ion batteries, *Journal of Energy Storage*, 2020, **29**, 101329.

7 J. Chen, M. N. Marlow, Q. Jiang and B. Wu, Peak-tracking method to quantify degradation modes in lithium-ion batteries via differential voltage and incremental capacity, *Journal of Energy Storage*, 2022, **45**, 103669.

8 X. Lu, M. Lagnoni, A. Bertei, S. Das, R. E. Owen, Q. Li, K. O'Regan, A. Wade, D. P. Finegan, E. Kendrick, M. Z. Bazant, D. J. L. Brett and P. R. Shearing, Multiscale dynamics of charging and plating in graphite electrodes coupling operando microscopy and phase-field modelling, *Nature communications*, 2023, **14**, 5127.

9 J. Schmitt, M. Schindler and A. Jossen, Change in the half-cell open-circuit potential curves of silicon–graphite and nickel-rich lithium nickel manganese cobalt oxide during cycle aging, *Journal of Power Sources*, 2021, **506**, 230240.

10 J. S. Edge, S. O'Kane, R. Prosser, N. D. Kirkaldy, A. N. Patel, A. Hales, A. Ghosh, W. Ai, J. Chen, J. Yang, S. Li, M.-C. Pang, L. Bravo Diaz, A. Tomaszewska, M. W. Marzook, K. N. Radhakrishnan, H. Wang, Y. Patel, B. Wu and G. J. Offer, Lithium ion battery degradation: what you need to know, *Physical chemistry chemical physics : PCCP*, 2021, **23**, 8200–8221.

11 X. Tang, Y. Wang, Q. Liu and F. Gao, Reconstruction of the incremental capacity trajectories from current-varying profiles for lithium-ion batteries, *iScience*, 2021, **24**, 103103.

12 W. Xu, J. Zhu, J. Zhang, M. Tian, J. Cai, H. Wu, G. Wei, T. Chen, X. Wei and H. Dai, Investigation of lithium-ion battery degradation by corrected differential voltage analysis based on reference electrode, *Applied Energy*, 2025, **389**, 125735.

13 B. Jiang, H. Dai and X. Wei, Incremental capacity analysis based adaptive capacity estimation for lithium-ion battery considering charging condition, *Applied Energy*, 2020, **269**, 115074.

14 X. Li, C. Yuan and Z. Wang, State of health estimation for Li-ion battery via partial incremental capacity analysis based on support vector regression, *Energy*, 2020, **203**, 117852.

15 A. Singh and A. Barai, Parametric investigation of partial incremental capacity analysis for Lithium-ion cells, *Journal of Energy Storage*, 2025, **113**, 115668.

16 H. Zhao, Q. Peng, X. Zheng and J. Meng, Unlocking minute-level battery incremental capacity analysis construction using deep learning and multi-sequence alignment, *Applied Energy*, 2025, **401**, 126763.

17 F. Wang, Z. Zhai, Z. Zhao, Y. Di and X. Chen, Physics-informed neural network for lithium-ion battery degradation stable modeling and prognosis, *Nature communications*, 2024, **15**, 4332.

18 Y. Tian, C. Lin, X. Meng, X. Yu, H. Li and R. Xiong, Accelerated commercial battery electrode-level degradation diagnosis via only 11-point charging segments, *eScience*, 2025, **5**, 100325.

19 S. Tao, J. Zhu, Y. Li, S. Chen, X. Wang, X. Wang, B. Jiang, W. Chang, X. Wei and H. Dai, State-of-health estimation for EV battery packs via incremental capacity curves and S-transform, *Applied Energy*, 2025, **397**, 126334.

20 J. Zhu, Y. Wang, Y. Huang, R. Bhushan Gopaluni, Y. Cao, M. Heere, M. J. Mühlbauer, L. Mereacre, H. Dai, X. Liu, A. Senyshyn, X. Wei, M. Knapp and H. Ehrenberg, Data-driven capacity estimation of commercial lithium-ion batteries from voltage relaxation, *Nature communications*, 2022, **13**, 2261.

21 C.-J. Ko and K.-C. Chen, Using tens of seconds of relaxation voltage to estimate open circuit voltage and state of health of lithium ion batteries, *Applied Energy*, 2024, **357**, 122488.

22 M. Schreiber, T. Steiner, J. Kayl, B. Schönberger, C. Grosu and M. Lienkamp, The Overlooked Role of Battery Cell Relaxation: How Reversible Effects Manipulate Accelerated Aging Characterization, *WEVJ*, 2025, **16**, 255.

23 X. Chen, Y. Hu, S. Li, Y. Wang, D. Li, C. Luo, X. Xue, F. Xu, Z. Zhang, Z. Gong, Y. Li and Y. Yang, State of health (SoH) estimation and degradation modes analysis of pouch NMC532/graphite Li-ion battery, *Journal of Power Sources*, 2021, **498**, 229884.

24 J. Sun and J. Kainz, A method to address the challenges of charging conditions on incremental capacity analysis: An ICA-compensation technique incorporating current

View Article Online
DOI: 10.1039/D6TA03434A

interrupt methods, *Journal of Energy Chemistry*, 2025, **108**, 65–80.

25 W. Zhang, R. Ahmed and S. Habibi, Understanding the impact of recent usage on lithium-ion battery impedance through the relaxation phenomena, *Journal of Power Sources*, 2025, **630**, 236108.

26 A. S. Ho, D. Y. Parkinson, S. E. Trask, A. N. Jansen and N. P. Balsara, Large Local Currents in a Lithium-Ion Battery during Rest after Fast Charging, *ACS nano*, 2023, **17**, 19180–19188.

27 S. P. Rangarajan, C. Fear, T. Adhikary, Y. Barsukov, G. Dadheech and P. P. Mukherjee, Dynamics of lithium stripping on graphite electrodes after fast charging, *Cell Reports Physical Science*, 2023, **4**, 101740.

28 L. Jahn, P. Mößle, F. Röder and M. A. Danzer, A physically motivated voltage hysteresis model for lithium-ion batteries using a probability distributed equivalent circuit, *Commun Eng*, 2024, **3**. DOI: 10.1038/s44172-024-00221-4.

29 Z. Chen, D. L. Danilov, L. H. Raijmakers, K. Chayambuka, M. Jiang, L. Zhou, J. Zhou, R.-A. Eichel and P. H. Notten, Overpotential analysis of graphite-based Li-ion batteries seen from a porous electrode modeling perspective, *Journal of Power Sources*, 2021, **509**, 230345.

30 A. Fernando, M. Kuipers, G. Angenendt, K.-P. Kairies and M. Dubarry, Benchmark dataset for the study of the relaxation of commercial NMC-811 and LFP cells, *Cell Reports Physical Science*, 2024, **5**, 101754.

31 S. Ma, M. Jiang, P. Tao, C. Song, J. Wu, J. Wang, T. Deng and W. Shang, Temperature effect and thermal impact in lithium-ion batteries: A review, *Progress in Natural Science: Materials International*, 2018, **28**, 653–666.

32 J. Guo, S. Jin, X. Sui, X. Huang, Y. Xu, Y. Li, P. K. Kristensen, D. Wang, K. Pedersen, L. Gurevich and D.-I. Stroe, Unravelling and quantifying the aging processes of commercial Li(Ni 0.5 Co 0.2 Mn 0.3)O 2 /graphite lithium-ion batteries under constant current cycling, *J. Mater. Chem. A*, 2022, **11**, 41–52.

33 J. Hemmerling, A. Fill and K. P. Birke, Analysis of the age-, current- and temperature-dependent expansion of cylindrical NCM | Graphite Li-ion battery cells using strain gauges, *Journal of Energy Storage*, 2024, **99**, 113177.

34 D. Ansean, V. M. Garcia, M. Gonzalez, C. Blanco-Viejo, J. C. Viera, Y. F. Pulido and L. Sanchez, Lithium-Ion Battery Degradation Indicators Via Incremental Capacity Analysis, *IEEE Trans. on Ind. Applicat.*, 2019, **55**, 2992–3002.

35 J. Guo, Y. Xu, Y. Liu, P. Li, Y. Che, Y. Li, K. Pedersen, G. Schuck, P. K. Kristensen, V. Baran, Y. Sun, P. Adelhelm and D.-I. Stroe, Degradation mechanisms of LiNi0.5Mn0.3Co0.2O2/graphite battery in real-life driving scenarios, *Energy Storage Materials*, 2025, **80**, 104441.

Protocol-aware standardization of relaxation-induced kinetic masking in incremental capacity fingerprints of lithium-ion batteries

DOI: 10.1039/D6TA03434A

Jinghua Sun[a,b] , *Yaolin Xu* *[a] *and Josef Kainz* [b,c]

[a] *Energy Materials & Interfaces (EMI) Group, Department of Applied Physics, Aalto University, Espoo, 00076 Finland*

[b] *Energy Technology, Technical University of Munich, Campus Straubing for Biotechnology and Sustainability, 94315 Straubing, Germany*

[c] *Weihenstephan-Triesdorf University of Applied Sciences, 94315 Straubing, Germany*

Data Availability Statement

Data for this article, including the processed reference performance test datasets, associated metadata, core MATLAB analysis code for the final leave-one-cell-out validation, and exported result tables, are available at Zenodo at https://doi.org/10.5281/zenodo.19705650.